

Enhancement of Intermediate-Field Two-Photon Absorption by Rationally-Shaped Femtosecond Pulses

Lev Chuntunov, Leonid Rybak, Andrey Gandman, and Zohar Amitay*

Schulich Faculty of Chemistry, Technion - Israel Institute of Technology, Haifa 32000, Israel

Abstract

We extend the powerful frequency-domain analysis of femtosecond two-photon absorption to the intermediate-field regime, which involves both two- and four-photon transitions. Consequently, we find a broad family of shaped pulses that enhance the absorption over the transform-limited pulse. It includes any spectral phase that is anti-symmetric around half the transition frequency. The spectrum is asymmetric around it. The theoretical framework and results for Na are verified experimentally. This work opens the door for rational femtosecond coherent control in a regime of considerable absorption yields.

PACS numbers: 31.15.Md, 32.80.Qk, 32.80.Wr, 42.65.Re

arXiv:0709.0486v1 [physics.atom-ph] 4 Sep 2007

*Electronic address: amitayz@tx.technion.ac.il

Following from their coherence over a broad spectrum, shaped femtosecond pulses allow to coherently control quantum dynamics in ways that other means cannot [1, 2, 3, 4, 5]. Among the processes, over which such control has been most effective, are the important multiphoton absorption processes [5, 6, 7, 8, 9, 10, 11, 12, 13, 14, 15, 16, 17, 18, 19]. The control is achieved by shaping the pulse to manipulate the interferences between various initial-to-final state-to-state multiphoton pathways. Constructive interferences enhance the absorption, while destructive interferences attenuate it. Thus, to fully utilize coherent control, the pulse shaping should ideally be based on identifying first the pathways and their interference mechanism. When such identification is not feasible, a practical partial solution is to employ automatic "black-box" experimental optimization of the pulse shape using learning algorithms [20]. For multiphoton processes, the past control studies [5, 6, 7, 8, 9, 10, 11, 12, 13, 14, 15] have shown that this ideal line of action is feasible and very powerful once the photo-excitation picture is available in the frequency domain. However, so far the frequency domain has been exploited only in the weak-field regime [5, 6, 7, 8, 9, 10, 11, 12, 13, 14, 15] associated with low absorption yields (typically up to $\sim 0.1\%$ population transfer). There, the N-photon absorption is described by time-dependent perturbation theory of the lowest non-vanishing order (the N^{th} order) and, thus, can be transformed to the frequency domain.

The present work extends the powerful frequency-domain picture to a regime of sizeable absorption yields, exceeding the weak-field yields by two orders of magnitude (and more). In this regime the interfering pathways of N-photon absorption are the weak-field pathways of N absorbed photons as well as additional pathways of M absorbed photons and M–N emitted photons ($M > N$). The corresponding picture is obtained by extending the perturbative analysis to include a finite number of non-vanishing orders beyond the lowest one. We refer to this regime as the intermediate-field regime. It is distinguished from the strong-field regime where no perturbative description is valid, which is the one all the past multiphoton control studies beyond the weak-field regime have focused on [16, 17, 18, 19]. Specifically, based on 4^{th} -order perturbation theory, we develop here an intermediate-field frequency-domain theoretical framework to the process of atomic femtosecond two-photon absorption, which is non-resonant in the weak-field regime (of 2^{nd} order). As a 4^{th} -order approach, it involves both the 2^{nd} and 4^{th} perturbative orders associated, respectively, with two- and four-photon pathways. Consequently, we find an extensive family of shaped pulses that in

this regime enhance the absorption as compared to the unshaped transform-limited (TL) pulse. This is impossible in the weak-field regime [6]. The theoretical framework and results are verified experimentally. The approach developed here is general and can be employed in other cases.

The physical model system of the study is the sodium (Na) atom (see Fig. 1). Theoretically, we consider an atomic two-photon absorption process from an initial ground state $|g\rangle$ to a final excited state $|f\rangle$, which are coupled via a manifold of intermediate states $|n\rangle$ having the proper symmetry. The spectrum of the pulse is such that all the $|g\rangle$ - $|n\rangle$ and $|f\rangle$ - $|n\rangle$ couplings are off-resonant, i.e., the spectral amplitude at all the corresponding transition frequencies is zero: $|E(\omega_{gn})| = |E(\omega_{fn})| = 0$, except for the $|f\rangle$ - $|n_r\rangle$ resonant coupling for which $|E(\omega_{fn_r})| \neq 0$. In the present intermediate-field regime, the final (complex) amplitude A_f of state $|f\rangle$, following irradiation with a (shaped) temporal electric field $\varepsilon(t)$, can be validly described by 4th-order time-dependent perturbation theory. So, in general, it includes non-vanishing contributions from both the 2nd and 4th perturbative orders:

$$A_f = A_f^{(2)} + A_f^{(4)}. \quad (1)$$

Within the frequency-domain framework, the spectral field $E(\omega) \equiv |E(\omega)| \exp[i\Phi(\omega)]$ is given as the Fourier transform of $\varepsilon(t)$, with $|E(\omega)|$ and $\Phi(\omega)$ being the spectral amplitude and phase at frequency ω . For the TL pulse: $\Phi(\omega) = 0$. We also introduce the normalized spectral field $\tilde{E}(\omega) \equiv E(\omega)/|E_0|$ representing the pulse shape, with $|E_0|$ being the maximal spectral amplitude. As shown for the weak-field regime [6], the 2nd-order term $A_f^{(2)}$ interferes all the $|g\rangle$ - $|f\rangle$ pathways of two absorbed photons (see examples in Fig. 1) and is given by

$$A_f^{(2)} = -\frac{1}{i\hbar^2} |E_0|^2 A^{(2)}(\omega_{fg}) \quad (2)$$

$$A^{(2)}(\Omega) = \mu_{fg}^2 \int_{-\infty}^{\infty} \tilde{E}(\omega) \tilde{E}(\Omega - \omega) d\omega, \quad (3)$$

where ω_{fg} and μ_{fg}^2 are the $|g\rangle$ - $|f\rangle$ transition frequency and effective non-resonant two-photon coupling. The TL pulse induces fully constructive interferences within $A_f^{(2)}$ and, thus, the maximal $|A_f^{(2)}|$ and maximal weak-field non-resonant two-photon absorption [6]. The 4th-order term $A_f^{(4)}$ is more complicated than $A_f^{(2)}$ and we have analytically calculated it to be given by

$$A_f^{(4)} = -\frac{1}{i\hbar^4} |E_0|^4 \left[i\pi A^{(2)}(\omega_{fg}) A^{(R)}(0) - \wp \int_{-\infty}^{\infty} d\delta \frac{1}{\delta} A^{(2)}(\omega_{fg} - \delta) A^{(R)}(\delta) \right], \quad (4)$$

where $A^{(2)}(\Omega)$ is defined above, and

$$A^{(R)}(\Delta\Omega) = A^{(\text{non-res}R)}(\Delta\Omega) + A^{(\text{res}R)}(\Delta\Omega) \quad (5)$$

$$A^{(\text{non-res}R)}(\Delta\Omega) = (\mu_{ff}^2 + \mu_{gg}^2) \int_{-\infty}^{\infty} \tilde{E}(\omega + \Delta\Omega) \tilde{E}^*(\omega) d\omega \quad (6)$$

$$A^{(\text{res}R)}(\Delta\Omega) = |\mu_{fr}|^2 \left[i\pi \tilde{E}(\omega_{fn_r} + \Delta\Omega) \tilde{E}^*(\omega_{fn_r}) - \wp \int_{-\infty}^{+\infty} d\delta' \frac{1}{\delta'} \tilde{E}(\omega_{fn_r} + \Delta\Omega - \delta') \tilde{E}^*(\omega_{fn_r} - \delta') \right]. \quad (7)$$

These equations reflect the fact that $A_f^{(4)}$ interferes all the four-photon pathways from $|g\rangle$ to $|f\rangle$ of any combination of three absorbed photons and one emitted photon.

Figure 1 shows several representative four-photon pathways. Each pathway can be divided into two parts: a non-resonant absorption of two photons with a frequency sum of $\Omega = \omega_{fg} - \delta$ and a Raman transition of two photons with a frequency difference of $\Delta\Omega = \delta$. Their border line is detuned by δ from either $|f\rangle$ or $|g\rangle$ according to whether, respectively, the two-photon absorption part or the Raman part comes first (see Fig. 1). The on-resonant ($\delta = 0$) and near-resonant ($\delta \neq 0$) pathways are interfered separately in Eq. (4). The Cauchy's principle value operator \wp excludes the on-resonant pathways from the second term. The integration over the pathways is expressed using two parameterized amplitudes, $A^{(2)}(\Omega)$ and $A^{(R)}(\Delta\Omega)$, that originate from the different parts of the four-photon pathways. $A^{(2)}(\Omega)$ interferes all the two-photon absorption pathways of frequency Ω . $A^{(R)}(\Delta\Omega)$ interferes all the Raman pathways of frequency $\Delta\Omega$ and includes two components. The first is $A^{(\text{non-res}R)}(\Delta\Omega)$ interfering all the Raman pathways that are non-resonant, with μ_{gg}^2 and μ_{ff}^2 being the $|g\rangle$ - $|g\rangle$ and $|f\rangle$ - $|f\rangle$ effective non-resonant Raman couplings due to the non-resonantly coupled states $|n\rangle$. The second is $A^{(\text{res}R)}(\Delta\Omega)$ interfering all the Raman pathways that are resonance-mediated via $|n_r\rangle$, with μ_{fn_r} being the $|f\rangle$ - $|n_r\rangle$ dipole matrix element.

For a given pulse shape $\tilde{E}(\omega)$, a non-zero $A_f^{(2)}$ is proportional to the maximal spectral intensity $I_0 = |E_0|^2$ while a non-zero $A_f^{(4)}$ is proportional to $I_0^2 = |E_0|^4$. Different intensity I_0 corresponds to a different temporal peak intensity of the TL pulse (I_{TL}). In this work, for a set of intensities I_0 , the $|f\rangle$'s final population $P_f = |A_f|^2$, which reflects the degree of two-photon absorption, is controlled via the pulse shape $\tilde{E}(\omega)$. The spectral phases $\Phi(\omega)$ are the corresponding control knobs, with the spectrum $|\tilde{E}(\omega)|$ unchanged. The latter is chosen such that the central frequency ω_0 is detuned from $\omega_{fg}/2$ and $|\tilde{E}(\omega_{fg}/2)|^2 \approx 0.5$. As discussed below, this corresponds to the interesting case of having $A_f^{(4)}$ negligible relative

to $A_f^{(2)}$ in the weak-field limit and comparable to $A_f^{(2)}$ in the upper intermediate-field limit. Their interplay enables the absorption enhancement beyond the TL absorption.

The Na system [22] includes the $3s$ ground state as $|g\rangle$, the $4s$ state as $|f\rangle$, the manifold of p states as the $|n\rangle$ manifold, and the $7p$ state as $|n_r\rangle$. The transition frequencies $\omega_{fg} \equiv \omega_{4s,3s}$ and $\omega_{fn_r} \equiv \omega_{7p,4s}$ correspond, respectively, to two 777-nm photons and one 781.2-nm photon. The sodium is irradiated with phase-shaped linearly-polarized femtosecond pulses having an intensity spectrum centered around 779.5 nm with 5 nm bandwidth (~ 180 fs TL duration). Experimentally, a sodium vapor in a heated cell is irradiated with such pulses of variable energy after they undergo shaping in an optical set-up with a pixelated liquid-crystal spatial light phase modulator [21]. Upon focusing, the TL temporal peak intensity at the peak of the spatial beam profile $I_{\text{TL}}^{(\text{profile-peak})}$ ranges from 10^9 to 5×10^{10} W/cm². Following the interaction with a pulse, the population excited to the $4s$ state undergoes cascaded decay to the $3s$ state via the $3p$ state. The corresponding $3p$ - $3s$ fluorescence serves as the relative measure for the final $4s$ population $P_f \equiv P_{4s}$. It is measured using a spectrometer coupled to a time-gated camera system. The measured signal results from an integration over the spatial beam profile.

We validate our intermediate-field frequency-domain perturbative description by comparing corresponding results to exact non-perturbative results obtained by the numerical propagation of the time-dependent Schrödinger equation (using the Runge-Kutta method). The considered manifold of p -states is from $3p$ to $8p$ [22]. The validity of the non-perturbative calculations is confirmed first by a comparison to experiment. The test case is the set of shaped pulses having a π -step spectral phase pattern. Each such pattern is characterized by the step position ω_{step} , with $\Phi(\omega \leq \omega_{step}) = -\pi/2$ and $\Phi(\omega > \omega_{step}) = \pi/2$. Figures 2(a)-(c) show examples of experimental (circles) and non-perturbative theoretical (solid lines) results of P_{4s} as a function of ω_{step} for different pulse energies, i.e., different $I_{\text{TL}}^{(\text{profile-peak})}$. Each of the traces is normalized by P_{4s} of the TL excitation. The weak-field trace [6] is shown in Fig. 2(a). The theoretical traces account for the experimental integration over the beam profile: Each of them results from a set of calculations conducted each with a different (single) value of I_0 . As can be seen, the agreement between the experimental and non-perturbative theoretical results is excellent, confirming these calculations' accuracy. Figs. 2(d)-(g) compare, for different (single-valued) intensities I_0 , the theoretical non-perturbative results (squares) with perturbative results calculated numerically using Eqs. (1)-(7) (solid lines). Shown are exam-

ples out of the full set of results. As can be seen, the perturbative results reproduce the non-perturbative ones up to the I_0 corresponding to a TL peak intensity of $I_{\text{TL}}=2.7\times 10^{10}$ W/cm² [Fig. 2(f)]. This is the intensity limit of the intermediate-field regime for the present Na excitation, up to which no perturbative order beyond the 4th one is needed to be included. The weak-field regime of $A_{4s}\approx A_{4s}^{(2)}$ extends here up to $I_{\text{TL}}\approx 10^9$ W/cm² [Fig. 2(d)].

As shown in Figs. 2(d)-(f), the π -trace shape significantly changes as I_0 increases. The prominent feature reflecting the deviation from the weak-field regime is the absorption enhancement beyond the TL absorption when ω_{step} is around $\omega_{4s,3s}/2$ (777 nm) or around the central spectral frequency ω_0 (780 nm). The enhancement increases as I_0 increases. Here, using the intermediate-field description, we analyze the enhancement mechanism when $\omega_{step} = \omega_{4s,3s}/2$. In the weak-field regime [Fig. 2(d)] the corresponding absorption is equal to the (maximal) TL absorption, since such a phase pattern also leads to fully constructive interferences within $A_{4s}^{(2)}$ [6]. In the present intermediate-field limit [Fig. 2(f)] it is about twice the TL absorption: With the I_0 of $I_{\text{TL}}=2.7\times 10^{10}$ W/cm² the calculated values are $\{A_{4s}^{(2)} = 0.35, A_{4s}^{(4)} = -0.15 - 0.10i : P_{4s} = 0.05\}$ for the TL pulse and $\{A_{4s}^{(2)} = 0.35, A_{4s}^{(4)} = -0.09 - 0.14i : P_{4s} = 0.09\}$ for the pulse of $\omega_{step} = \omega_{4s,3s}/2$. So, as seen from these values, the lower TL absorption results mainly from a stronger attenuation of the equal real $A_{4s}^{(2)}$ by $\Re[A_{4s}^{(4)}]$.

The difference in $\Re[A_{4s}^{(4)}]$ for these two pulses originates from the \wp -integral in Eq. (4), which interferes all the near-resonant four-photon pathways of $\delta \neq 0$ with the domination of small $|\delta|$ (due to the $1/\delta$ weighting). Actually, it predominantly originates from the integrand factor $A^{(2)}(\omega_{4s,3s} - \delta)$ interfering all the two-photon absorption parts (of these four-photon pathways) of transition frequency $\omega_{4s,3s} - \delta$. For the TL pulse, due to fully constructive interferences, $A^{(2)}(\omega_{4s,3s} - \delta)$ is maximized (real and positive value) for any δ . So, with a detuned spectrum of $\omega_0 \neq \omega_{4s,3s}/2$, it changes monotonically with δ around $\delta = 0$. $A^{(2)}(\omega_{4s,3s} - |\delta|) > A^{(2)}(\omega_{4s,3s} + |\delta|)$ with a red spectral detuning, and vice versa with a blue detuning. On the other hand, for the shaped pulse of $\omega_{step}=\omega_{4s,3s}/2$, $A^{(2)}(\omega_{4s,3s} - \delta)$ is maximized only for $\delta = 0$ and gradually reduces for small non-zero $|\delta|$ with comparable magnitude for $\pm|\delta|$ (true for both red and blue spectral detuning). Consequently, considering also the $1/\delta$ integrand factor, the \wp -integral results in a higher value of $|\Re[A_{4s}^{(4)}]|$ for the TL pulse. For both pulses, the sign of $\Re[A_{4s}^{(4)}]$ relative to $A_{4s}^{(2)}$ is determined by the pulse spectrum and by the Raman couplings of the four-photon pathways ($\mu_{3s,3s}^2$, $\mu_{4s,4s}^2$ and $|\mu_{4s,7p}|^2$). Here,

the present red-detuned spectrum (ω_0 of 779.5 nm) leads to $A_{4s}^{(2)}$ and $\Re[A_{4s}^{(4)}]$ that are of opposite signs. Shifting the spectrum to be comparably blue detuned from $\omega_{4s,3s}/2$ (ω_0 of 774.5 nm) changes their signs to be the same. Then, the intermediate-field absorption of the TL pulse is the higher one. A non-detuned spectrum (ω_0 of 777 nm) leads to a negligible $\Re[A_{4s}^{(4)}]$ and thus to an equal absorption for both pulses, in agreement with the strong-field time-domain study by Dudovich *et al.* [16]. This spectral dependence is the subject of future publication. For the current red-detuning, the above explanation also allows to understand why the enhancement over the TL absorption increases as I_0 increases: Since $|\Re[A_{4s}^{(4)}]|/A_{4s}^{(2)} = KI_0$ with higher value of K for the TL pulse as compared to the shaped pulse of $\omega_{step}=\omega_{4s,3s}/2$, a given increase of I_0 results in a higher increase in the attenuation of $A_{4s}^{(2)}$ by $A_{4s}^{(4)}$ for the TL pulse.

Similar to the π -step phase pattern of $\omega_{step}=\omega_{4s,3s}/2$, all the spectral phase patterns that are anti-symmetric around $\omega_{4s,3s}/2$, i.e., $\Phi(\omega) = -\Phi(\omega_{4s,3s} - \omega)$, lead to the maximal weak-field two-photon absorption for, and only for, a transition frequency of $\omega_{4s,3s}$ [6]. So, based on the above analysis, in the intermediate-field regime the corresponding shaped pulses are expected to enhance the two-photon absorption (to the 4s state) beyond the TL absorption. The mechanism is the enhanced attenuation of $A_{4s}^{(2)}$ by $A_{4s}^{(4)}$ for the TL pulse. Figure 3 confirms that indeed this is the case. It shows theoretical [Fig. 3(a)] and experimental [Fig. 3(b)] results for 5000 different pulse shapes with such anti-symmetric phase patterns that we have randomized. The results are presented as histograms (distributions) showing the fraction of pulses inducing different values of $P_{4s}/P_{4s}^{(TL)}$, i.e., different absorption enhancement over to the TL excitation. The theoretical results are perturbative and have been calculated numerically using Eqs. (1)-(7), with each histogram corresponding to a different (single-valued) intensity I_0 . The (spatially-integrated) experimental histograms correspond to different pulse energies. The weak-field histogram is located at the value of 1.

As can be seen, the distribution shifts to higher enhancement values and gets broader as I_0 increases. Both effects originate from the I_0 -dependence of $|\Re[A_{4s}^{(4)}]|/A_{4s}^{(2)} = KI_0$, with K depending only on the pulse shape. Similar to the $\omega_{step}=\omega_{4s,3s}/2$ case, the shift to higher enhancement values originates from the higher K value for the TL pulse as compared to the shaped pulses with the anti-symmetric phase patterns. The distribution broadening originates from the variation in the K value from one pulse shape to the other. The experimental histograms are generally broader than the theoretical ones due to the integration over the

spatial beam profile and due to the experimental noise. The experimental signal-to-noise ratio is directly reflected in the width of the weak-field histogram [Fig. 3(b)-dashed line]. Our most-enhancing random anti-symmetric pattern is calculated at I_0 of $I_{\text{TL}}=2.7\times 10^{10}$ W/cm² to induce $P_{4s}=0.21$, corresponding to 4.2 enhancement over the TL absorption. Last, it worth mentioning that excluding the resonantly-coupled $7p$ state from our calculations generally leads to about 25% reduction in the enhancement factors over the TL absorption at $I_{\text{TL}}=2.7\times 10^{10}$ W/cm².

In summary, we have extended the powerful frequency-domain analysis of femtosecond two-photon absorption to the intermediate-field regime of 2nd and 4th perturbative orders. This opens the door for rational femtosecond coherent control beyond the weak-field regime, in a regime of considerable absorption yields. The extended frequency-domain description has enabled us to identify a broad family of shaped pulses that enhance the absorption beyond the TL absorption. The mechanism is the coherent interplay between the different perturbative orders. We expect this work to serve as a basis for intermediate-field extensions to molecules and other multiphoton processes as well as for devising effective control strategies when several multiphoton channels are involved. The results are also of applicative importance for nonlinear spectroscopy and microscopy.

-
- [1] D. J. Tannor, R. Kosloff, and S. A. Rice, *J. Chem. Phys.* **85**, 5805 (1986).
 - [2] M. Shapiro and P. Brumer, *Principles of the quantum control of molecular processes* (Wiley, New Jersey, 2003).
 - [3] W. S. Warren, H. Rabitz, and D. Mahleh, *Science* **259**, 1581 (1993).
 - [4] H. Rabitz, R. de Vivie-Riedle, M. Motzkus, and K. Kompa, *Science* **288**, 824 (2000).
 - [5] M. Dantus and V. V. Lozovoy, *Chem. Rev.* **104**, 1813 (2004); *ChemPhysChem* **6**, 1970 (2005).
 - [6] D. Meshulach and Y. Silberberg, *Nature (London)* **396**, 239 (1998); *Phys. Rev. A* **60**, 1287 (1999).
 - [7] K. A. Walowicz *et al.*, *J. Phys. Chem. A* **106**, 9369 (2002); V. V. Lozovoy *et al.*, *J. Chem. Phys.* **118**, 3187 (2003).
 - [8] A. Präkelt *et al.*, *Phys. Rev. A* **70**, 063407 (2004).
 - [9] N. Dudovich *et al.*, *Phys. Rev. Lett.* **86**, 47 (2001).

- [10] B. Chatel, J. Degert, and B. Girard, *Phys. Rev. A* **70**, 053414 (2004).
- [11] P. Panek and A. Becker, *Phys. Rev. A* **74**, 023408 (2006).
- [12] D. Oron *et al.*, *Phys. Rev. A* **65**, 043408 (2002); N. Dudovich, D. Oron, and Y. Silberberg, *Nature (London)* **418**, 512 (2002);
- [13] H. U. Stauffer *et al.*, *J. Chem. Phys.* **116**, 946 (2002); X. Dai, E. W. Lerch, and S. R. Leone, *Phys. Rev. A* **73**, 023404 (2006).
- [14] A. Gandman, L. Chuntunov, L. Rybak, and Z. Amitay, *Phys. Rev. A* **75**, 031401 (R) (2007).
- [15] E. Gershgoren *et al.*, *Opt. Lett.* **28**, 361 (2003).
- [16] N. Dudovich *et al.*, *Phys. Rev. Lett.* **94**, 083002 (2005).
- [17] C. Trallero-Herrero *et al.*, *Phys. Rev. A* **71**, 013423 (2005); *Phys. Rev. Lett.* **96**, 063603 (2006).
- [18] M. Wollenhaupt *et al.*, *Phys. Rev. A* **68**, 015401 (2003); *Phys. Rev. A* **73**, 063409 (2006);
- [19] S. A. Hosseini and D. Goswami, *Phys. Rev. A* **64**, 033410 (2001).
- [20] R. Judson and H. Rabitz, *Phys. Rev. Lett.* **68**, 1500 (1992).
- [21] A. M. Weiner, *Rev. Sci. Inst.* **71**, 1929 (2000).
- [22] NIST Atomic Spectra Database (National Institute of Standards and Technology, Gaithersburg, MD).

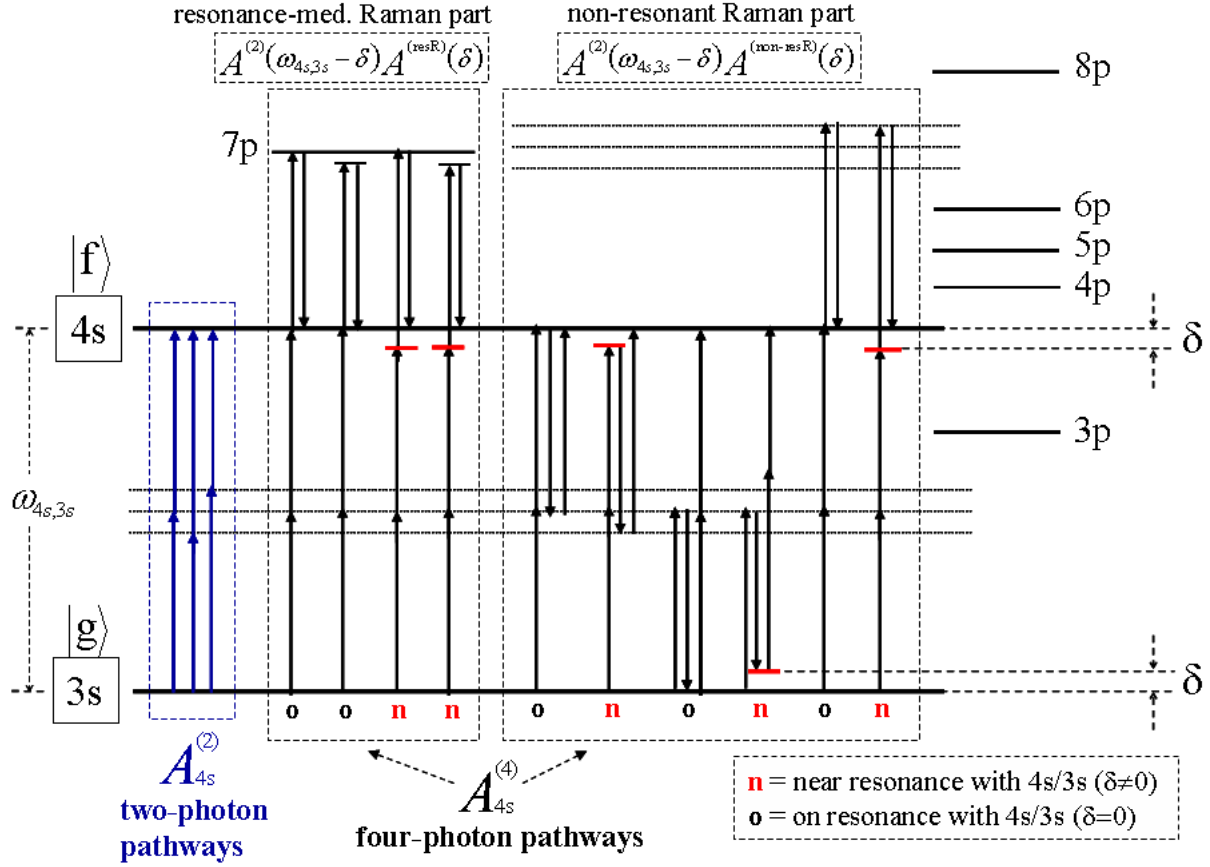


FIG. 1: (Color online) Excitation scheme of the intermediate-field two-photon absorption in Na (not to scale), with representative two-photon and four-photon pathways from $|g\rangle \equiv 3s$ to $|f\rangle \equiv 4s$. Each of the four-photon pathways is either on- or near-resonance with $4s$ or $3s$. Its Raman part is non-resonant due to the np states ($n \neq 7$) or resonance-mediated via $7p$.

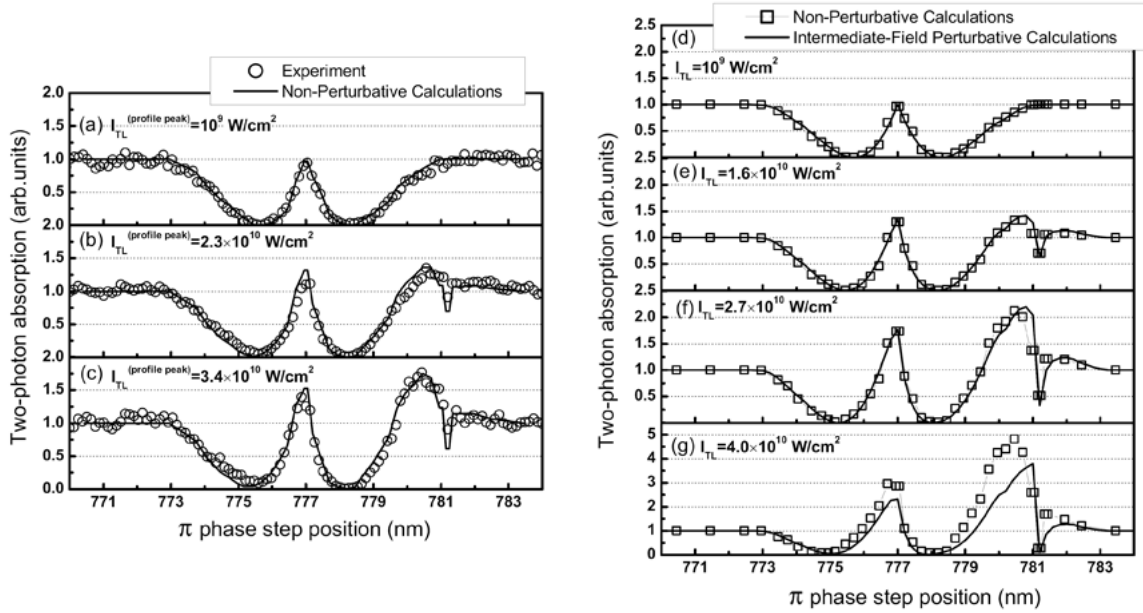


FIG. 2: Results for the Na two-photon absorption induced by the shaped pulses with a π spectral phase step as a function of the step position. Panels (a)-(c): Experimental (circles) and non-perturbative theoretical (solid lines) results (spatially integrated) for different pulse energies corresponding to a TL intensity at the peak of the spatial beam profile $I_{\text{TL}}^{(\text{profile-peak})}$ of (a) 10^9 , (b) 2.3×10^{10} , and (c) 3.4×10^{10} W/cm². Panels (d)-(g): Non-perturbative (squares) and perturbative (solid lines) theoretical results for different (single-valued) spectral intensities I_0 (see text) corresponding to a TL intensity I_{TL} of (d) 10^9 , (e) 1.6×10^{10} , (f) 2.7×10^{10} , and (g) 4×10^{10} W/cm². The perturbative calculations include 2nd and 4th orders.

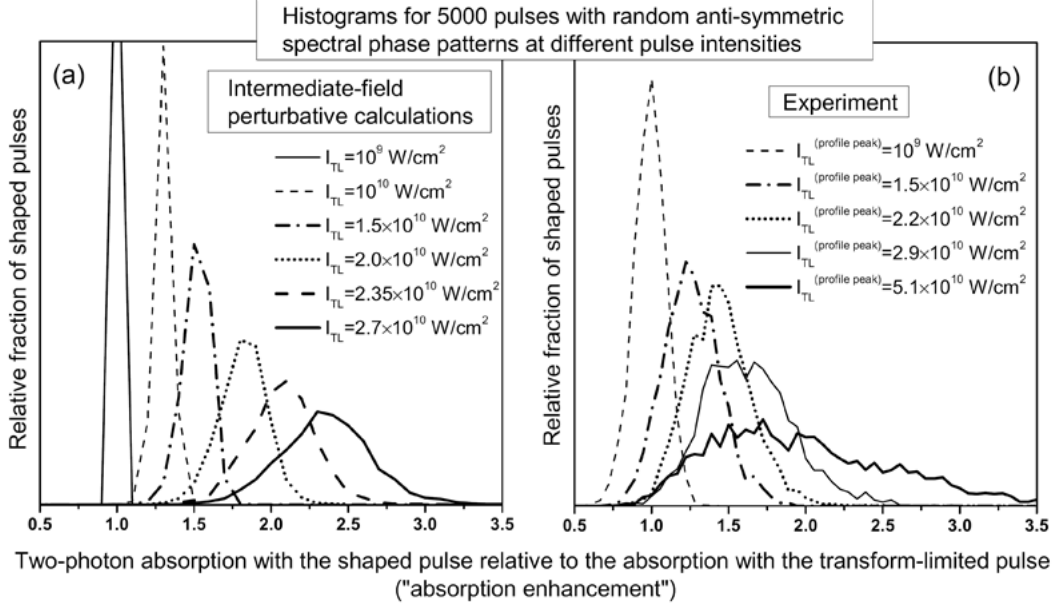


FIG. 3: Histograms of the Na two-photon absorption for a set of 5000 different pulses with random spectral phase patterns that are all anti-symmetric around $\omega_{4s,3s}/2$. They show the fraction of pulses inducing different absorption enhancement over the TL pulse. (a) Theoretical perturbative results (of 2nd and 4th orders) for different (single-valued) spectral intensities I_0 corresponding to different TL intensities I_{TL} . (b) Experimental results (spatially integrated) for different pulse energies corresponding to different TL intensities at the peak of the beam profile $I_{TL}^{(\text{profile-peak})}$.